

# First Measurement of Energy-dependent Inclusive Muon Neutrino Charged-Current Cross Sections on Argon with the MicroBooNE Detector

P. Abratenko,<sup>33</sup> R. An,<sup>14</sup> J. Anthony,<sup>4</sup> L. Arellano,<sup>18</sup> J. Asaadi,<sup>32</sup> A. Ashkenazi,<sup>30</sup> S. Balasubramanian,<sup>11</sup> B. Baller,<sup>11</sup> C. Barnes,<sup>20</sup> G. Barr,<sup>23</sup> V. Basque,<sup>18</sup> L. Bathe-Peters,<sup>13</sup> O. Benevides Rodrigues,<sup>29</sup> S. Berkman,<sup>11</sup> A. Bhandari,<sup>18</sup> A. Bhat,<sup>29</sup> M. Bishai,<sup>2</sup> A. Blake,<sup>16</sup> T. Bolton,<sup>15</sup> J. Y. Book,<sup>13</sup> L. Camilleri,<sup>9</sup> D. Caratelli,<sup>11</sup> I. Caro Terrazas,<sup>8</sup> F. Cavanna,<sup>11</sup> G. Cerati,<sup>11</sup> Y. Chen,<sup>1</sup> D. Cianci,<sup>9</sup> J. M. Conrad,<sup>19</sup> M. Convery,<sup>26</sup> L. Cooper-Troendle,<sup>36</sup> J. I. Crespo-Anadón,<sup>5</sup> M. Del Tutto,<sup>11</sup> S. R. Dennis,<sup>4</sup> P. Detje,<sup>4</sup> A. Devitt,<sup>16</sup> R. Diurba,<sup>21</sup> R. Dorrill,<sup>14</sup> K. Duffy,<sup>11</sup> S. Dytman,<sup>24</sup> B. Eberly,<sup>28</sup> A. Ereditato,<sup>1</sup> J. J. Evans,<sup>18</sup> R. Fine,<sup>17</sup> G. A. Fiorentini Aguirre,<sup>27</sup> R. S. Fitzpatrick,<sup>20</sup> B. T. Fleming,<sup>36</sup> N. Foppiani,<sup>13</sup> D. Franco,<sup>36</sup> A. P. Furmanski,<sup>21</sup> D. Garcia-Gamez,<sup>12</sup> S. Gardiner,<sup>11</sup> G. Ge,<sup>9</sup> S. Gollapinni,<sup>31,17</sup> O. Goodwin,<sup>18</sup> E. Gramellini,<sup>11</sup> P. Green,<sup>18</sup> H. Greenlee,<sup>11</sup> W. Gu,<sup>2</sup> R. Guenette,<sup>13</sup> P. Guzowski,<sup>18</sup> L. Hagaman,<sup>36</sup> O. Hen,<sup>19</sup> C. Hilgenberg,<sup>21</sup> G. A. Horton-Smith,<sup>15</sup> A. Hourlier,<sup>19</sup> R. Itay,<sup>26</sup> C. James,<sup>11</sup> X. Ji,<sup>2</sup> L. Jiang,<sup>34</sup> J. H. Jo,<sup>36</sup> R. A. Johnson,<sup>7</sup> Y.-J. Jwa,<sup>9</sup> D. Kalra,<sup>9</sup> N. Kamp,<sup>19</sup> N. Kaneshige,<sup>3</sup> G. Karagiorgi,<sup>9</sup> W. Ketchum,<sup>11</sup> M. Kirby,<sup>11</sup> T. Kobilarcik,<sup>11</sup> I. Kreslo,<sup>1</sup> I. Lepetic,<sup>25</sup> K. Li,<sup>36</sup> Y. Li,<sup>2</sup> K. Lin,<sup>17</sup> B. R. Littlejohn,<sup>14</sup> W. C. Louis,<sup>17</sup> X. Luo,<sup>3</sup> K. Manivannan,<sup>29</sup> C. Mariani,<sup>34</sup> D. Marsden,<sup>18</sup> J. Marshall,<sup>35</sup> D. A. Martinez Caicedo,<sup>27</sup> K. Mason,<sup>33</sup> A. Mastbaum,<sup>25</sup> N. McConkey,<sup>18</sup> V. Meddage,<sup>15</sup> T. Mettler,<sup>1</sup> K. Miller,<sup>6</sup> J. Mills,<sup>33</sup> K. Mistry,<sup>18</sup> A. Mogan,<sup>31</sup> T. Mohayai,<sup>11</sup> J. Moon,<sup>19</sup> M. Mooney,<sup>8</sup> A. F. Moor,<sup>4</sup> C. D. Moore,<sup>11</sup> L. Mora Lepin,<sup>18</sup> J. Mousseau,<sup>20</sup> M. Murphy,<sup>34</sup> D. Naples,<sup>24</sup> A. Navrer-Agasson,<sup>18</sup> M. Nebot-Guinot,<sup>10</sup> R. K. Neely,<sup>15</sup> D. A. Newmark,<sup>17</sup> J. Nowak,<sup>16</sup> M. Nunes,<sup>29</sup> O. Palamara,<sup>11</sup> V. Paolone,<sup>24</sup> A. Papadopoulou,<sup>19</sup> V. Papavassiliou,<sup>22</sup> S. F. Pate,<sup>22</sup> N. Patel,<sup>16</sup> A. Paudel,<sup>15</sup> Z. Pavlovic,<sup>11</sup> E. Piasetzky,<sup>30</sup> I. D. Ponce-Pinto,<sup>36</sup> S. Prince,<sup>13</sup> X. Qian,<sup>2</sup> J. L. Raaf,<sup>11</sup> V. Radeka,<sup>2</sup> A. Raffique,<sup>15</sup> M. Reggiani-Guzzo,<sup>18</sup> L. Ren,<sup>22</sup> L. C. J. Rice,<sup>24</sup> L. Rochester,<sup>26</sup> J. Rodriguez Rondon,<sup>27</sup> M. Rosenberg,<sup>24</sup> M. Ross-Lonergan,<sup>9</sup> G. Scanavini,<sup>36</sup> D. W. Schmitz,<sup>6</sup> A. Schukraft,<sup>11</sup> W. Seligman,<sup>9</sup> M. H. Shaevitz,<sup>9</sup> R. Sharankova,<sup>33</sup> J. Shi,<sup>4</sup> J. Sinclair,<sup>1</sup> A. Smith,<sup>4</sup> E. L. Snider,<sup>11</sup> M. Soderberg,<sup>29</sup> S. Söldner-Rembold,<sup>18</sup> P. Spentzouris,<sup>11</sup> J. Spitz,<sup>20</sup> M. Stancari,<sup>11</sup> J. St. John,<sup>11</sup> T. Strauss,<sup>11</sup> K. Sutton,<sup>9</sup> S. Sword-Fehlberg,<sup>22</sup> A. M. Szelc,<sup>10</sup> W. Tang,<sup>31</sup> K. Terao,<sup>26</sup> C. Thorpe,<sup>16</sup> D. Totani,<sup>3</sup> M. Touns,<sup>11</sup> Y.-T. Tsai,<sup>26</sup> M. A. Uchida,<sup>4</sup> T. Usher,<sup>26</sup> W. Van De Pontseele,<sup>23,13</sup> B. Viren,<sup>2</sup> M. Weber,<sup>1</sup> H. Wei,<sup>2</sup> Z. Williams,<sup>32</sup> S. Wolbers,<sup>11</sup> T. Wongjirad,<sup>33</sup> M. Wospakrik,<sup>11</sup> K. Wresilo,<sup>4</sup> N. Wright,<sup>19</sup> W. Wu,<sup>11</sup> E. Yandel,<sup>3</sup> T. Yang,<sup>11</sup> G. Yarbrough,<sup>31</sup> L. E. Yates,<sup>19</sup> H. W. Yu,<sup>2</sup> G. P. Zeller,<sup>11</sup> J. Zennaro,<sup>11</sup> and C. Zhang<sup>2</sup>

(The MicroBooNE Collaboration)\*

<sup>1</sup>Universität Bern, Bern CH-3012, Switzerland

<sup>2</sup>Brookhaven National Laboratory (BNL), Upton, NY, 11973, USA

<sup>3</sup>University of California, Santa Barbara, CA, 93106, USA

<sup>4</sup>University of Cambridge, Cambridge CB3 0HE, United Kingdom

<sup>5</sup>Centro de Investigaciones Energéticas, Medioambientales y Tecnológicas (CIEMAT), Madrid E-28040, Spain

<sup>6</sup>University of Chicago, Chicago, IL, 60637, USA

<sup>7</sup>University of Cincinnati, Cincinnati, OH, 45221, USA

<sup>8</sup>Colorado State University, Fort Collins, CO, 80523, USA

<sup>9</sup>Columbia University, New York, NY, 10027, USA

<sup>10</sup>University of Edinburgh, Edinburgh EH9 3FD, United Kingdom

<sup>11</sup>Fermi National Accelerator Laboratory (FNAL), Batavia, IL 60510, USA

<sup>12</sup>Universidad de Granada, Granada E-18071, Spain

<sup>13</sup>Harvard University, Cambridge, MA 02138, USA

<sup>14</sup>Illinois Institute of Technology (IIT), Chicago, IL 60616, USA

<sup>15</sup>Kansas State University (KSU), Manhattan, KS, 66506, USA

<sup>16</sup>Lancaster University, Lancaster LA1 4YW, United Kingdom

<sup>17</sup>Los Alamos National Laboratory (LANL), Los Alamos, NM, 87545, USA

<sup>18</sup>The University of Manchester, Manchester M13 9PL, United Kingdom

<sup>19</sup>Massachusetts Institute of Technology (MIT), Cambridge, MA, 02139, USA

<sup>20</sup>University of Michigan, Ann Arbor, MI, 48109, USA

<sup>21</sup>University of Minnesota, Minneapolis, MN, 55455, USA

<sup>22</sup>New Mexico State University (NMSU), Las Cruces, NM, 88003, USA

<sup>23</sup>University of Oxford, Oxford OX1 3RH, United Kingdom

<sup>24</sup>University of Pittsburgh, Pittsburgh, PA, 15260, USA

<sup>25</sup>Rutgers University, Piscataway, NJ, 08854, USA

<sup>26</sup>SLAC National Accelerator Laboratory, Menlo Park, CA, 94025, USA

<sup>27</sup>South Dakota School of Mines and Technology (SDSMT), Rapid City, SD, 57701, USA

<sup>28</sup>University of Southern Maine, Portland, ME, 04104, USA

<sup>29</sup>Syracuse University, Syracuse, NY, 13244, USA

<sup>30</sup>*Tel Aviv University, Tel Aviv, Israel, 69978*

<sup>31</sup>*University of Tennessee, Knoxville, TN, 37996, USA*

<sup>32</sup>*University of Texas, Arlington, TX, 76019, USA*

<sup>33</sup>*Tufts University, Medford, MA, 02155, USA*

<sup>34</sup>*Center for Neutrino Physics, Virginia Tech, Blacksburg, VA, 24061, USA*

<sup>35</sup>*University of Warwick, Coventry CV4 7AL, United Kingdom*

<sup>36</sup>*Wright Laboratory, Department of Physics, Yale University, New Haven, CT, 06520, USA*

(Dated: October 28, 2021)

We report a measurement of the energy-dependent total charged-current cross section  $\sigma(E_\nu)$  for inclusive muon neutrinos scattering on argon, as well as measurements of flux-averaged differential cross sections as a function of muon energy and hadronic energy transfer ( $\nu$ ). Data corresponding to  $5.3 \times 10^{19}$  protons on target of exposure were collected using the MicroBooNE liquid argon time projection chamber located in the Fermilab Booster Neutrino Beam with a mean neutrino energy of approximately 0.8 GeV. The mapping between the true neutrino energy  $E_\nu$  and reconstructed neutrino energy  $E_\nu^{rec}$  and between the energy transfer  $\nu$  and reconstructed hadronic energy  $E_{had}^{rec}$  are validated by comparing the data and Monte Carlo (MC) predictions. In particular, the modeling of the missing hadronic energy and its associated uncertainties are verified by a new method that compares the  $E_{had}^{rec}$  distributions between data and an MC prediction after constraining the reconstructed muon kinematic distributions, energy and polar angle, to those of data. The success of this validation gives confidence that the missing energy in the MicroBooNE detector is well-modeled and underpins first-time measurements of both the total cross section  $\sigma(E_\nu)$  and the differential cross section  $d\sigma/d\nu$  on argon.

Current and next-generation precision neutrino oscillation experiments aim to answer several critical questions in particle physics [1] by: i) searching for CP violation in the lepton sector [2, 3], ii) determining the neutrino mass ordering [4], and iii) searching for light sterile neutrinos [5]. For this purpose, the SBN [6] and DUNE [7, 8] experiments employ liquid argon time projection chambers (LArTPCs) [9–12], a tracking calorimeter that enables excellent neutrino flavor identification and neutrino energy ( $E_\nu$ ) reconstruction in the GeV energy range [13]. These experiments are designed to measure the neutrino flavor oscillations as a function of  $E_\nu$ , which requires a good understanding of the neutrino energy spectrum, neutrino-argon interaction cross sections [14], and LArTPC detector response. High-precision measurements of  $\nu$ -Ar cross sections, particularly those related to energy reconstruction, are of paramount importance.

While historical accelerator-based neutrino experiments often reported  $E_\nu$ -dependent cross sections [15, 16], recent experiments tend to limit cross-section measurements to the directly observable lepton and/or hadron kinematics [17]. This paradigm shift was triggered by concerns that quantities not directly measurable in detectors (e.g. the missing hadronic energy of the interaction from undetected neutral particles) may not be correctly modeled in simulations, which is of particular concern in a broad-band neutrino beam. In this letter, we demonstrate that the MicroBooNE tune model [18] (based on GENIE-v3 [19]) of missing energy with its associated uncertainty can be validated with inclusive muon neutrino charged-current ( $\nu_\mu$ CC) interactions from the the MicroBooNE detector [20]. After constraining the

lepton kinematics distributions of Monte Carlo (MC) to those of data, the comparison of reconstructed hadronic energy  $E_{had}^{rec}$  distributions between data and the updated MC prediction reveals whether the model is able to describe the relationship between the lepton kinematics and the visible hadronic energy. This procedure validates whether the missing hadronic energy is sufficiently modelled given the prior knowledge of the neutrino flux and detector effects. This new procedure enables a first measurement of the differential cross section as a function of the energy transfer to the argon  $d\sigma/d\nu$ . Together with the differential cross section as a function of the muon energy ( $d\sigma/dE_\mu$ ), the  $E_\nu$ -dependent cross sections are extracted. These data could be used to isolate problems for low- $E_\nu$  cross sections and to reduce modelling uncertainties for the low- $\nu$  method [21–23] to constrain the shape of neutrino energy spectrum in future experiments.

The MicroBooNE detector is a  $10.4 \times 2.6 \times 2.3$  m<sup>3</sup> LArTPC. It consists of approximately 85 ton of LAr in the active TPC volume for ionization charge detection, along with 32 photomultiplier tubes (PMTs) [24] for scintillation light detection. This work makes use of a data set corresponding to an exposure of  $5.3 \times 10^{19}$  protons on target (POT) from the Booster Neutrino Beamline (BNB), which produces a neutrino flux with an estimated 93.6%  $\nu_\mu$  purity [25] and a mean  $E_\nu$  of 0.8 GeV. At these energies,  $\nu$ -Ar interactions are dominated by quasi-elastic and meson-exchange current interactions, and the final-state hadrons consist mostly of protons and neutrons with some charged and neutral pions. The  $\mathcal{O}(1)$  MeV energy threshold [26] of LArTPC allows detecting these particles down to low kinetic energies.

Compared to earlier work [27], this measurement incorporates an improved TPC detector simulation and signal processing procedure [28, 29], the Wire-Cell tomographic event reconstruction [30, 31], and a many-to-many TPC-

---

\* microboone\_info@fnal.gov

charge to PMT-light matching algorithm for cosmic-ray rejection [31]. In particular, the “generic neutrino detection” [32, 33], which limits the cosmic-ray muon backgrounds to below 15% at over 80%  $\nu_\mu$ CC selection efficiency, is used as a pre-selection. The  $\nu_\mu$ CC event selection is further improved using a set of pattern recognition techniques, including i) neutrino vertex identification, ii) track/shower topology separation, iii) particle identification, and iv) particle flow reconstruction in the Wire-Cell reconstruction package [34, 35].

First, the reconstructed neutrino vertex is required to be inside a fiducial volume, defined to be 3 cm inside the effective detector boundary [33]. Second, a set of dedicated background taggers are constructed to further reject residual muon backgrounds that entered the detector from outside based on directional information. Finally, neutral-current (NC) events are substantially reduced by requiring a reconstructed primary muon candidate to be longer than 5 cm. Some limited charged pion rejection is achieved by detecting large-angle scattering in reconstructed track trajectories. Using input variables from the background taggers, a multivariate classifier is constructed using the modern boosted decision tree (BDT) library XGBoost [36] that yields a  $\nu_\mu$ CC selection with an estimated 92% purity and 68% efficiency. In total, 11528  $\nu_\mu$ CC candidates are selected and used for cross-section extraction. About 1/3 of the events are fully contained (FC) and 2/3 are partially contained (PC). Here, the FC events are defined to be events with their main TPC cluster [31] fully contained within the fiducial volume [33] and PC events are mostly because of exiting muons.

Three methods are used to reconstruct the energy of tracks and electromagnetic (EM) showers [34, 35]: i) The energy of a stopped charged particle track can be estimated by its travel *range* using the NIST PSTAR database [37]. ii) The kinetic energy of a charged particle track can be estimated by integrating over the reconstructed energy loss per unit length  $dE/dx$ , which is calculated from the measured  $dQ/dx$  (ionization charge per unit length) using a *recombination* model [38]. iii) The energy of an EM shower can be estimated calorimetrically by *scaling* the total reconstructed charge of the EM shower with a factor of 2.50, which is derived from simulation and includes the bias in the reconstructed charge [31] and the average recombination factor. This factor is validated with the reconstructed invariant mass of the neutral pion [39]. For stopping tracks with trajectories longer than 4 cm, the *range* method is used to estimate the energy. For short tracks (<4 cm), tracks exiting the detector, tracks with “wiggled” topology [34] (e.g. low-energy electrons), and muon tracks with identified  $\delta$  rays, the *recombination* method is used to estimate its kinetic energy.

The reconstructed neutrino energy  $E_\nu^{rec}$  per event is estimated by summing the kinetic energies of each reconstructed (visible) final-state particle. For each reconstructed muon, charged pion, or electron candidate, its mass is added to the energy reconstruction. An average

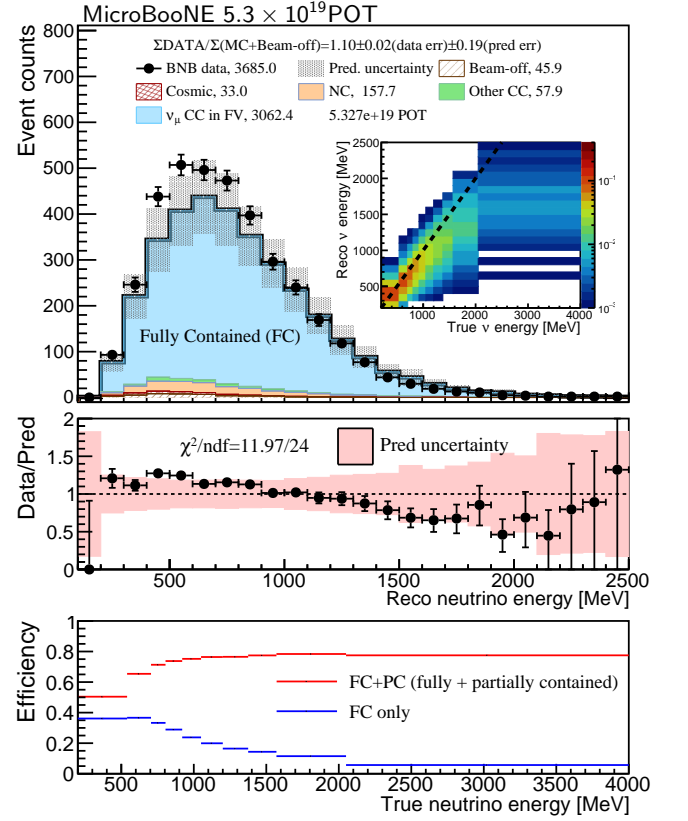


FIG. 1. (Top) Distribution of the selected FC  $\nu_\mu$ CC events as a function of reconstructed neutrino energy. The inset figure is the smearing matrix from true neutrino energy to reconstructed neutrino energy. (Middle) Data/prediction ratio. The pink band represents the total uncertainty (statistical and systematic) of the MC prediction. (Bottom) Selection efficiency of the  $\nu_\mu$ CC events in the fiducial volume as a function of true neutrino energy.

binding energy of 8.6 MeV was added for each proton identified. Figure 1 shows the FC  $\nu_\mu$ CC distribution as a function of reconstructed neutrino energy, the selection efficiency as a function of true neutrino energy, and the smearing matrix between  $E_\nu^{rec}$  and  $E_\nu$  according to the Monte Carlo simulation. The predicted energy resolution for FC  $\nu_\mu$ CC events is  $\sim 10\%$  for muon energy,  $\sim 20\%$  for neutrino energy, and  $\sim 30\text{--}50\%$  for hadronic energy. The hadronic energy resolution is dominated by the missing hadronic energy and imperfect event reconstruction. For events well reconstructed, the resolution of the reconstructed visible hadronic energy approaches  $\sim 10\%$ . Among all events, the average bias (towards low energy) of  $E_\nu^{rec}$  for FC  $\nu_\mu$ CC events is less than 10% for  $E_\nu < 800$  MeV and increases to  $\sim 25\%$  at  $E_\nu = 2.5$  GeV.

The total and differential cross sections are extracted using the Wiener-SVD unfolding method [40] as follows:

$$M_i - B_i = \sum_j R_{ij} \cdot S_j = \sum_j \tilde{\Delta}_{ij} \cdot \tilde{F}_j \cdot S_j. \quad (1)$$

$M_i$  is the measured number of events in bin  $i$  of the re-

constructed energy space, and  $B_i$  is the expected number of backgrounds.  $R_{ij} = \tilde{\Delta}_{ij} \cdot \bar{F}_j$  is the overall response matrix.  $S_j$ , to be extracted, is the average (differential) cross section in bin  $j$  of the true energy, weighted by the nominal  $\nu_\mu$  neutrino flux, which is tabulated in Ref. [27]. This definition of  $S_j$  with the nominal neutrino flux naturally resolves one recent concern on the treatment of neutrino flux uncertainty [41].  $\tilde{\Delta}_{ij}$ , the ratio between the selected number of events in reconstructed energy bin  $i$  that originate from the true energy bin  $j$  and the generated number of events in bin  $j$ , is calculated using central-value MC. This encapsulates both the smearing between reconstructed and true space and the efficiency.  $\bar{F}_j$  is a constant that is calculated with the POT, number of Ar nuclei, the integrated nominal  $\nu_\mu$  flux in bin  $j$ , and the bin width (for differential cross sections only).

The Wiener-SVD unfolding is performed based on a

$$\chi^2 = (\mathbf{M} - \mathbf{B} - \mathbf{R} \cdot \mathbf{S})^T \cdot \mathbf{V}^{-1} \cdot (\mathbf{M} - \mathbf{B} - \mathbf{R} \cdot \mathbf{S}) \quad (2)$$

test statistics and an additional regularization constructed from a Wiener filter [40], where  $\mathbf{V}$  is the covariance matrix on the measured number of events in the reconstructed energy bins, encoding the statistical and systematic uncertainties. Statistical uncertainties on the data are calculated following the combined Neyman Pearson procedure [42]. The covariance matrix also includes i) statistical uncertainties on the simulation [43]; ii) uncertainties on the neutrino flux model [27]; iii) uncertainties on the neutrino-argon interaction cross section model [18] based on GENIE v3.0.6 [19]. The uncertainties associated with the hadronic interactions, which are important in modeling missing energy, are conservatively estimated. The proton to neutron charge exchange and the proton knockout have 50% and 20% uncertainties, respectively; iv) uncertainties on the GEANT4 models used to simulate hadron-argon interactions [44, 45] outside the target nucleus; v) uncertainties on the detector model; vi) uncertainties on the modeling of “dirt” events that originate outside the cryostat; vii) uncertainties on the POT (2% based on *in-situ* proton flux measurements [25]); and viii) uncertainties on the number of target nuclei ( $\sim 1\%$ ). The uncertainties on the neutrino flux (5-15%), neutrino-argon cross section ( $\sim 20\%$ ), and hadron-argon interaction ( $\sim 1.5\%$ ) models are estimated using a *multisim* technique [46].

The uncertainties on the detector model include i) variations in the TPC waveform, ii) variations related to the light yield and propagation, iii) variation in the space charge effect [47, 48], and iv) variation in the ionization recombination model. For each source, the same set of MC interactions are re-simulated through the detector response simulation with a  $1\sigma$  change to the corresponding detector model parameter. The differences in the selected number of events between the modified and original simulations are used to construct a covariance matrix with a bootstrapping [49] procedure. Although the uncertainty on the predicted inclusive cross section is  $\sim 20\%$ , given Eq. (1), the cross section enters through both numerator

and denominator of  $\tilde{\Delta}_{ij}$  as well as  $B_i$ , reducing its uncertainty contribution to  $\sim 5\%$ . In comparison, the uncertainties on the neutrino flux, GEANT4 model, detector model, and POT enter through  $B_i$  and the numerator of  $\tilde{\Delta}_{ij}$ . “Dirt” uncertainties enter through  $B_i$ .

A prior condition of using the Wiener-SVD unfolding method to extract cross sections is that the data must be well-described by the overall model prediction within its uncertainties. In Fig. 1 and Fig. 2, data and simulation are shown for key reconstructed kinematic variables including i) neutrino energy  $E_\nu^{rec}$ , ii) muon energy  $E_\mu^{rec}$ , iii) cosine of muon polar angle  $\cos\theta_\mu^{rec}$ , and iv) hadronic energy  $E_{had}^{rec}$ . The compatibility between the data and prediction is demonstrated quantitatively by decent  $\chi^2/\text{ndf}$  values (ndf is the number of degrees of freedom) considering full uncertainties using the Pearson  $\chi^2$  [50]. To examine different components of systematic uncertainties, we further utilize the conditional covariance matrix formalism [51] to adjust the model prediction and reduce its uncertainties by applying constraints from data. Figure 2a) shows the comparison of the  $E_\mu^{rec}$  distribution for PC  $\nu_\mu\text{CC}$  in data to that of the model prediction after applying constraints from the FC  $E_\mu^{rec}$  events. While the uncertainties are largely reduced, there is only a small change to  $\chi^2/\text{ndf}$ . The data and constrained model agree within uncertainties, verifying the modeling of the invisible energy of muons outside the active detector volume for PC events. Figure 2b) shows the comparison of the  $\cos\theta_\mu^{rec}$  distribution for both FC and PC  $\nu_\mu\text{CC}$  candidates in data with the model prediction after applying a constraint from the  $E_\mu^{rec}$  distributions of the same set of  $\nu_\mu\text{CC}$  candidate events. Compared to the previous case, the correlated statistical uncertainties between the  $\cos\theta_\mu^{rec}$  distributions and the  $E_\mu^{rec}$  distributions are estimated with a bootstrapping procedure. While the uncertainties are significantly reduced after applying the constraint, the change to  $\chi^2/\text{ndf}$  is small, showing well-modeled muon kinematics.

We will examine the modeling of the mapping between the reconstructed energy of the hadronic system  $E_{had}^{rec}$  and the energy transfer to the argon nucleus  $\nu = E_\nu - E_\mu$  after taking into account the muon results. The mapping of  $E_{had}^{rec}$  to  $\nu$  (or  $E_\nu^{rec}$  to true  $E_\nu$ ) relies on the overall cross section model to correct for the missing energy going into undetected neutrons, low-energy photons and other particles below the detection threshold. To validate the model, we examine the  $E_{had}^{rec}$  distribution for the FC  $\nu_\mu\text{CC}$  candidates in data with that of the model prediction after applying constraints from two one-dimensional distributions in muon kinematics:  $E_\mu^{rec}$  and  $\cos\theta_\mu^{rec}$  in Fig. 2c). After applying constraints, the uncertainties on the model prediction for  $E_{had}^{rec}$  are significantly reduced because of the cancellation of common systematic uncertainties, such as neutrino flux. At the lowest energies, it reduces from 20% to 5%. Nevertheless, the  $\chi^2/\text{ndf}$  values are still below one, indicating that the model describes the relationship between  $E_{had}^{rec}$  and  $E_\mu^{rec}$  well within its uncertainty. In particular, the difference between the

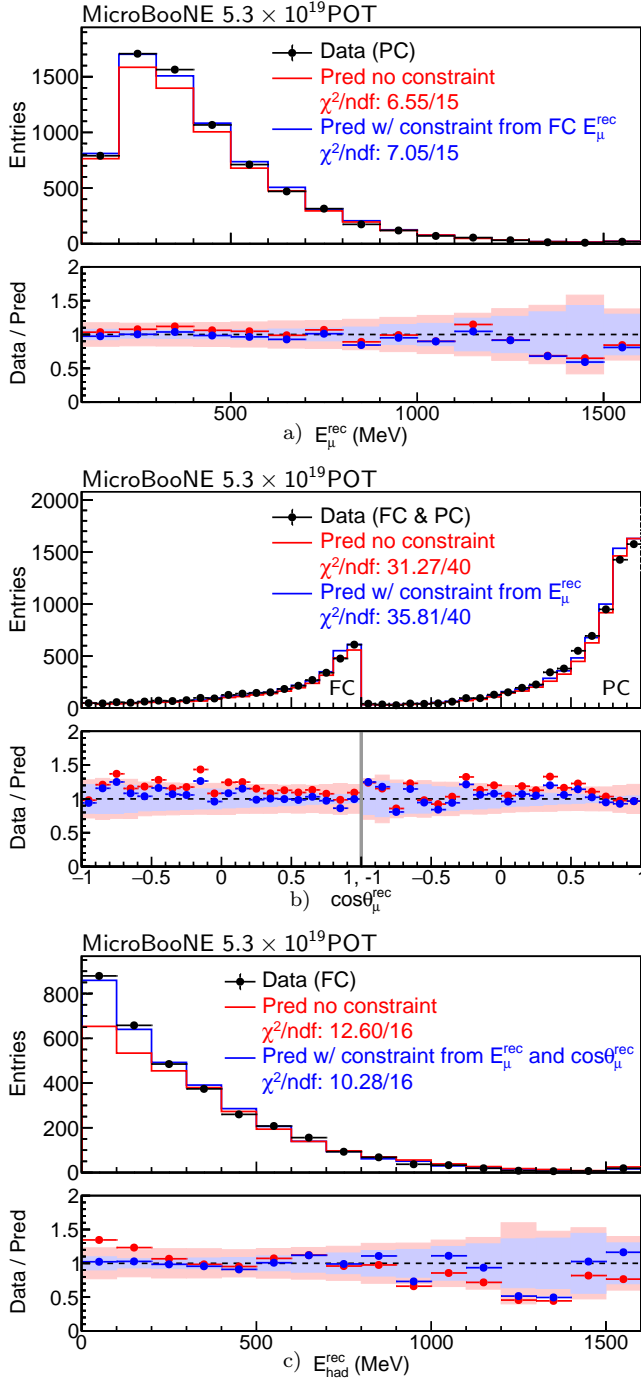


FIG. 2. Data are compared with MC predictions as a function of: a) reconstructed muon energy  $E_\mu^{rec}$  for the partially contained (PC) sample. The MC prediction after applying constraints from the fully-contained (FC) sample in  $E_\mu^{rec}$  is shown. The last bin represents all events with  $E_\mu^{rec} > 1.5$  GeV. The blue (red) points represent the ratio between data and the MC prediction with (without) constraint, and the bands with same colors depict the total (include statistical) uncertainty of the MC prediction. b) reconstructed  $\cos \theta_\mu^{rec}$  for the FC (first half) and PC (second half) sample. The MC prediction after applying constraints on both FC and PC samples in  $E_\mu^{rec}$  is shown. c) reconstructed hadronic energy  $E_{had}^{rec}$  for the FC sample. The MC prediction after applying constraints on muon kinematics ( $E_\mu^{rec}$  and  $\cos \theta_\mu^{rec}$ ) is shown. The last bin represents all events with  $E_{had}^{rec} > 1.5$  GeV.

data and the model prediction in the first three bins of  $E_{had}^{rec}$  is significantly reduced after applying the constraints. This test further validates that the modeling of the missing hadronic energy can describe data within its associated uncertainty. We note the conditional covariance matrix formalism, which is used to update the MC predictions and their uncertainties given the data constraints, is only used in validating the overall model [35], and is not used in extracting cross sections through the unfolding procedure. With fake data, we show that the  $\chi^2/ndf$  has a significant increase with a shift of  $\sim 15\%$  in the hadronic energy fraction allocated to protons (mimicking a variation of the proton-inelastic cross section), and this procedure is also able to distinguish between two GENIE models.

With the overall model validated, the total and differential cross sections per nucleon are extracted. The binning of the unfolded results is chosen by considering the energy resolution and the number of samples in the true space. The total cross section divided by the bin-center neutrino energy is shown as a function of neutrino energy in Fig. 3a), where the bin-center is calculated as the flux-weighted average neutrino energy. Besides the nominal cross-section model used in the “MicroBooNE MC” [18], predictions from GENIE v3.0.6 [19, 52], NuWro 19.02.01 [53], NEUT 5.4.0.1 [54], and GiBUU 2019.08 [55] after applying the Wiener filter are quantitatively compared with the measurement through calculating  $\chi^2/ndf$  with the uncertainty covariance matrix obtained from the unfolding procedure. Note that these comparisons only incorporate the central predictions from various generators without their theoretical uncertainties, which are particularly important in constructing predictions in analysis. The central predictions of GENIE v3 and NuWro are disfavored compared to the other three. Particularly, the “MicroBooNE MC” (tuned GENIE-v3 model [18]) has better agreement than GENIE v3.0.6, given the tuned GENIE-v3 model is constructed by fitting T2K data [56] in a similar energy range.

Figure 3b) and c) show the flux-averaged differential cross sections as a function of muon energy ( $d\sigma/dE_\mu$ ) and energy transfer to the argon nucleus ( $d\sigma/d\nu$ ). The same set of model predictions are compared to these measurements. The model comparison of  $d\sigma/dE_\mu$  shows a shape agreement with most models, although the normalization predictions differ. The central predictions of GENIE v3 and NuWro are more disfavored. The model predictions in  $d\sigma/d\nu$  show large variations, particularly in the low energy transfer ( $\nu$ ) region, where the shape difference contributes considerably to the  $\chi^2/ndf$  given the correlations in the uncertainty covariance matrix. The central prediction from GiBUU has the best agreement with data in the low  $\nu$  region, but is systematically lower than data at high  $\nu$  region. Considering all three cross-section results, the GiBUU prediction has the best agreement with acceptable  $\chi^2/ndf$  values, while the performance of the NEUT prediction is comparable. The central predictions of the other three models show larger disagreement.

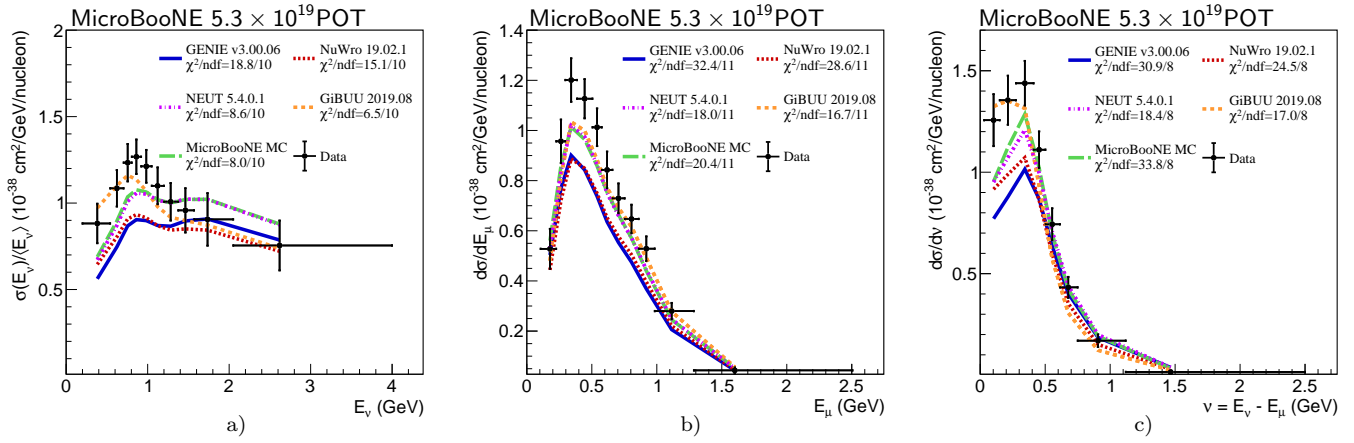


FIG. 3. a) The extracted  $\nu_\mu$ CC inclusive scattering cross section per nucleon divided by the bin-center neutrino energy, as a function of neutrino energy. b) The measured  $\nu_\mu$ CC differential cross section per nucleon as a function of muon energy  $d\sigma/dE_\mu$ . c) The measured  $\nu_\mu$ CC differential cross section per nucleon as a function of energy transfer  $d\sigma/d\nu$ . Various model predictions are compared to all three measurements (see text for details).

In summary, we present a measurement of cross section as a function of the neutrino energy based on data from a broad-band neutrino beam. We report the nominal-flux weighted total inclusive  $\nu_\mu$ CC cross sections  $\sigma(E_\nu)$ , and the nominal flux-averaged differential cross sections as a function of muon energy  $d\sigma/dE_\mu$  and energy transfer  $d\sigma/d\nu$  using the Wiener-SVD unfolding method [40]. A new procedure based on the conditional covariance matrix formalism [51] and the bootstrapping method [49] is used to validate the model of missing energies, which enables the first measurement of  $d\sigma/d\nu$  on argon and significantly adds value to the measurement of the total cross section as function of neutrino energy  $\sigma(E_\nu)$ . These results provide a detailed way to compare data and calculations beyond what is possible with existing flux-averaged total cross section results. With additional accumulated data statistics (up to  $1.2 \times 10^{21}$  POT from BNB) in the MicroBooNE detector, additional neutrino cross-section measurements are expected that will lead to further model development and generator improvements for neutrino scattering in argon.

## ACKNOWLEDGMENTS

This document was prepared by the MicroBooNE collaboration using the resources of the Fermi National Ac-

celerator Laboratory (Fermilab), a U.S. Department of Energy, Office of Science, HEP User Facility. Fermilab is managed by Fermi Research Alliance, LLC (FRA), acting under Contract No. DE-AC02-07CH11359. MicroBooNE is supported by the following: the U.S. Department of Energy, Office of Science, Offices of High Energy Physics and Nuclear Physics; the U.S. National Science Foundation; the Swiss National Science Foundation; the Science and Technology Facilities Council (STFC), part of the United Kingdom Research and Innovation; the Royal Society (United Kingdom); and The European Union's Horizon 2020 Marie Skłodowska-Curie Actions. Additional support for the laser calibration system and cosmic ray tagger was provided by the Albert Einstein Center for Fundamental Physics, Bern, Switzerland. We also acknowledge the contributions of technical and scientific staff to the design, construction, and operation of the MicroBooNE detector as well as the contributions of past collaborators to the development of MicroBooNE analyses, without whom this work would not have been possible.

- 
- [1] M. V. Diwan, V. Galymov, X. Qian, and A. Rubbia, “Long-Baseline Neutrino Experiments,” *Ann. Rev. Nucl. Part. Sci.* **66**, 47–71 (2016).
  - [2] K. Abe *et al.* (T2K), “Improved constraints on neutrino mixing from the T2K experiment with  $3.13 \times 10^{21}$  protons on target,” *Phys. Rev. D* **103**, 112008 (2021), arXiv:2101.03779 [hep-ex].
  - [3] M. A. Acero *et al.* (NOvA), “An Improved Measurement of Neutrino Oscillation Parameters by the NOvA Experiment,” (2021), arXiv:2108.08219 [hep-ex].
  - [4] X. Qian and P. Vogel, “Neutrino Mass Hierarchy,” *Prog. Part. Nucl. Phys.* **83**, 1–30 (2015).



- [5] Pedro AN Machado, Ornella Palamara, and David W Schmitz, “The Short-Baseline Neutrino Program at Fermilab,” *Ann. Rev. Nucl. Part. Sci.* **69** (2019).
- [6] M. Antonello *et al.* (MicroBooNE, LAr1-ND, ICARUS-WA104), “A Proposal for a Three Detector Short-Baseline Neutrino Oscillation Program in the Fermilab Booster Neutrino Beam,” (2015), arXiv:1503.01520 [physics.ins-det].
- [7] R. Acciarri *et al.* (DUNE Collaboration), “Long-Baseline Neutrino Facility (LBNF) and Deep Underground Neutrino Experiment (DUNE),” (2016), arXiv:1601.05471 [physics.ins-det].
- [8] Babak Abi *et al.* (DUNE), “Deep Underground Neutrino Experiment (DUNE), Far Detector Technical Design Report, Volume I Introduction to DUNE,” *JINST* **15**, T08008 (2020), arXiv:2002.02967 [physics.ins-det].
- [9] C. Rubbia, “The Liquid Argon Time Projection Chamber: A New Concept for Neutrino Detectors,” CERN-EP-INT-77-08, CERN-EP-77-08 (1977).
- [10] H. H. Chen, P. E. Condon, B. C. Barish, and F. J. Sciulli, “A Neutrino detector sensitive to rare processes. I. A Study of neutrino electron reactions,” *FERMILAB-PROPOSAL-0496* (1976).
- [11] W.J. Willis and V. Radeka, “Liquid Argon Ionization Chambers as Total Absorption Detectors,” *Nucl. Instrum. Meth.* **120**, 221–236 (1974).
- [12] D.R. Nygren, “The Time Projection Chamber: A New 4 pi Detector for Charged Particles,” *eConf* **C740805**, 58 (1974).
- [13] F. Cavanna, A. Ereditato, and B. T. Fleming, “Advances in liquid argon detectors,” *Nucl. Instrum. Meth.* **A907**, 1–8 (2018).
- [14] J. A. Formaggio and G. P. Zeller, “From eV to EeV: Neutrino Cross Sections Across Energy Scales,” *Rev. Mod. Phys.* **84**, 1307–1341 (2012), arXiv:1305.7513 [hep-ex].
- [15] P. Adamson *et al.* (MINOS), “Neutrino and Antineutrino Inclusive Charged-current Cross Section Measurements with the MINOS Near Detector,” *Phys. Rev. D* **81**, 072002 (2010), arXiv:0910.2201 [hep-ex].
- [16] A. A. Aguilar-Arevalo *et al.* (MiniBooNE), “Measurement of Neutrino-Induced Charged-Current Charged Pion Production Cross Sections on Mineral Oil at  $E_\nu \sim 1$  GeV,” *Phys. Rev. D* **83**, 052007 (2011), arXiv:1011.3572 [hep-ex].
- [17] P. A. Zyla *et al.* (Particle Data Group), “Review of Particle Physics (Section 51),” *PTEP* **2020**, 083C01 (2020).
- [18] P. Abratenko *et al.* (MicroBooNE), “New Theory-driven GENIE Tune for MicroBooNE,” [https://microboone.fnal.gov/genie\\_tune\\_2021/](https://microboone.fnal.gov/genie_tune_2021/) (2021).
- [19] Luis Alvarez-Ruso *et al.* (GENIE), “Recent highlights from GENIE v3,” (2021), arXiv:2106.09381 [hep-ph].
- [20] R. Acciarri *et al.* (MicroBooNE Collaboration), “Design and Construction of the MicroBooNE Detector,” *JINST* **12**, P02017 (2017).
- [21] S. R. Mishra, in *Proceedings of the Workshop on Hadron Structure Functions and Parton Distributions*, edited by D. Geesaman *et al.*
- [22] W. Seligman, Ph.D. thesis, Columbia University, 1997, Nevis 292.
- [23] A. Bodek, U. Sarica, D. Naples, and L. Ren, “Methods to Determine Neutrino Flux at Low Energies: Investigation of the Low  $\nu$  Method,” *Eur. Phys. J. C* **72**, 1973 (2012), arXiv:1201.3025 [hep-ex].
- [24] J. Conrad *et al.*, “The Photomultiplier Tube Calibration System of the MicroBooNE Experiment,” *JINST* **10** (2015), 10.1088/1748-0221/10/06/T06001, arXiv:1502.04159 [physics.ins-det].
- [25] A. A. Aguilar-Arevalo *et al.* (MiniBooNE), “The Neutrino Flux prediction at MiniBooNE,” *Phys. Rev. D* **79**, 072002 (2009), arXiv:0806.1449 [hep-ex].
- [26] R. Acciarri *et al.* (ArgoNeuT), “Demonstration of MeV-Scale Physics in Liquid Argon Time Projection Chambers Using ArgoNeuT,” *Phys. Rev. D* **99**, 012002 (2019), arXiv:1810.06502 [hep-ex].
- [27] P. Abratenko *et al.* (MicroBooNE Collaboration), “First Measurement of Inclusive Muon Neutrino Charged Current Differential Cross Sections on Argon at  $E_\nu \sim 0.8$  GeV with the MicroBooNE Detector,” *Phys. Rev. Lett.* **123**, 131801 (2019).
- [28] C. Adams *et al.* (MicroBooNE Collaboration), “Ionization electron signal processing in single phase LArTPCs. Part I. Algorithm Description and quantitative evaluation with MicroBooNE simulation,” *JINST* **13**, P07006–P07006 (2018).
- [29] C. Adams *et al.* (MicroBooNE Collaboration), “Ionization electron signal processing in single phase LArTPCs. Part II. Data/simulation comparison and performance in MicroBooNE,” *JINST* **13**, P07007 (2018).
- [30] Xin Qian, Chao Zhang, Brett Viren, and Milind Diwan, “Three-dimensional Imaging for Large LArTPCs,” *JINST* **13**, P05032 (2018).
- [31] P. Abratenko *et al.* (MicroBooNE), “Neutrino event selection in the MicroBooNE liquid argon time projection chamber using Wire-Cell 3D imaging, clustering, and charge-light matching,” *JINST* **16**, P06043 (2021), arXiv:2011.01375 [physics.ins-det].
- [32] P. Abratenko *et al.* (MicroBooNE), “High-performance Generic Neutrino Detection in a LArTPC near the Earth’s Surface with the MicroBooNE Detector,” (2020), arXiv:2012.07928 [hep-ex].
- [33] P. Abratenko *et al.* (MicroBooNE), “Cosmic Ray Background Rejection with Wire-Cell LArTPC Event Reconstruction in the MicroBooNE Detector,” *Phys. Rev. Applied* **15**, 064071 (2021), arXiv:2101.05076 [physics.ins-det].
- [34] P. Abratenko *et al.* (MicroBooNE), “Wire-Cell 3D Pattern Recognition Techniques for Neutrino Event Reconstruction in large LArTPCs: Algorithm Description and Quantitative Evaluation with MicroBooNE Simulation,” (2021), in preparation.
- [35] P. Abratenko *et al.* (MicroBooNE), “Search for an anomalous excess of inclusive charged-current  $\nu_e$  interactions in the MicroBooNE experiment using Wire-Cell reconstruction,” [https://microboone.fnal.gov/electron\\_analysis\\_1ex\\_2021/](https://microboone.fnal.gov/electron_analysis_1ex_2021/) (2021).
- [36] Tianqi Chen and Carlos Guestrin, “XGBoost: A Scalable Tree Boosting System,” (2016), 10.1145/2939672.2939785, arXiv:1603.02754 [cs.LG].
- [37] PSTAR at NIST: <https://physics.nist.gov/PhysRefData/Star/Text/PSTAR.html>.
- [38] C. Adams *et al.* (MicroBooNE Collaboration), “Calibration of the Charge and Energy Response of the MicroBooNE Liquid Argon Time Projection Chamber using Muons and Protons,” *JINST* **15**, P03022 (2020).
- [39] C. Adams *et al.* (MicroBooNE Collaboration), “Reconstruction and Measurement of  $\mathcal{O}(100)$  MeV Energy Electromagnetic Activity from  $\pi^0 \rightarrow \gamma\gamma$  Decays in the MicroBooNE LArTPC,” *JINST* **15**, P02007 (2020).

- [40] W. Tang, X. Li, X. Qian, H. Wei, and C. Zhang, “Data Unfolding with Wiener-SVD Method,” JINST **12**, P10002 (2017), arXiv:1705.03568 [physics.data-an].
- [41] Lukas Koch and Stephen Dolan, “Treatment of flux shape uncertainties in unfolded, flux-averaged neutrino cross-section measurements,” Phys. Rev. D **102**, 113012 (2020), arXiv:2009.00552 [hep-ex].
- [42] Xiangpan Ji, Wenqiang Gu, Xin Qian, Hanyu Wei, and Chao Zhang, “Combined Neyman–Pearson chi-square: An improved approximation to the Poisson-likelihood chi-square,” Nucl. Instrum. Meth. A **961**, 163677 (2020), arXiv:1903.07185 [physics.data-an].
- [43] Carlos A. Argüelles, Austin Schneider, and Tianlu Yuan, “A binned likelihood for stochastic models,” JHEP **06**, 030 (2019), arXiv:1901.04645 [physics.data-an].
- [44] J. Allison *et al.*, “Recent developments in Geant4,” Nucl. Instrum. Meth. A **835**, 186–225 (2016).
- [45] J. Calcutt, C. Thorpe, K. Mahn, and Laura Fields, “Geant4Reweight: a framework for evaluating and propagating hadronic interaction uncertainties in Geant4,” JINST **16**, P08042 (2021), arXiv:2105.01744 [physics.data-an].
- [46] Byron P Roe, “Statistical errors in monte carlo estimates of systematic errors,” Nuclear Instruments and Methods in Physics Research Section A: Accelerators, Spectrometers, Detectors and Associated Equipment **570**, 159–164 (2007).
- [47] P. Abratenko *et al.* (MicroBooNE), “Measurement of space charge effects in the MicroBooNE LArTPC using cosmic muons,” JINST **15**, P12037 (2020), arXiv:2008.09765 [physics.ins-det].
- [48] C. Adams *et al.* (MicroBooNE Collaboration), “A Method to Determine the Electric Field of Liquid Argon Time Projection Chambers Using a UV Laser System and its Application in MicroBooNE,” JINST **15**, P07010 (2020).
- [49] Bradley Efron and Robert J. Tibshirani, *An Introduction to the Bootstrap*, Monographs on Statistics and Applied Probability No. 57 (Chapman & Hall/CRC, Boca Raton, Florida, USA, 1993).
- [50] T. Hauschild and M. Jentschel, “Comparison of maximum likelihood estimation and chi-square statistics applied to counting experiments,” Nucl. Instrum. Meth. **A457**, 384–401 (2001).
- [51] Morris L Eaton, “Multivariate statistics: a vector space approach,” John Wiley and Sons, 116–117 (1983).
- [52] C. Andreopoulos *et al.*, “The GENIE Neutrino Monte Carlo Generator,” Nucl. Instrum. Meth. A **614**, 87–104 (2010), arXiv:0905.2517 [hep-ph].
- [53] T. Golan, J. T. Sobczyk, and J. Zmuda, “NuWro: the Wroclaw Monte Carlo Generator of Neutrino Interactions,” Nucl. Phys. B Proc. Suppl. **229–232**, 499–499 (2012).
- [54] Yoshinari Hayato, “A neutrino interaction simulation program library NEUT,” Acta Phys. Polon. B **40**, 2477–2489 (2009).
- [55] O. Buss, T. Gaitanos, K. Gallmeister, H. van Hees, M. Kaskulov, O. Lalakulich, A. B. Larionov, T. Leitner, J. Weil, and U. Mosel, “Transport-theoretical Description of Nuclear Reactions,” Phys. Rept. **512**, 1–124 (2012), arXiv:1106.1344 [hep-ph].
- [56] Ko Abe *et al.* (T2K), “Measurement of double-differential muon neutrino charged-current interactions on C<sub>8</sub>H<sub>8</sub> without pions in the final state using the T2K off-axis beam,” Phys. Rev. D **93**, 112012 (2016), arXiv:1602.03652 [hep-ex].